

Optimized multichannel quantum defect theory for cold molecular collisions

James F. E. Croft and Jeremy M. Hutson

Joint Quantum Centre (JQC) Durham/Newcastle, Department of Chemistry, Durham University, South Road, Durham, DH1 3LE, United Kingdom

Paul S. Julienne

Joint Quantum Institute, National Institute of Standards and Technology, and the University of Maryland, Gaithersburg, Maryland 20899-8423, USA

(Received 26 June 2012; published 20 August 2012)

Multichannel quantum defect theory (MQDT) can provide an efficient alternative to full coupled-channel calculations for low-energy molecular collisions. However, the efficiency relies on interpolation of the Y matrix that encapsulates the short-range dynamics, and there are poles in Y that may prevent interpolation over the range of energies of interest for cold molecular collisions. We show how the phases of the MQDT reference functions may be chosen so as to remove such poles from the vicinity of a reference energy and dramatically increase the range of interpolation. For the test case of Mg + NH, the resulting optimized Y matrix may be interpolated smoothly over an energy range of several Kelvin and a magnetic field range of over 1000 gauss. Calculations at additional energies and fields can then be performed at a computational cost that is proportional to the number of channels N and not to N^3 .

DOI: [10.1103/PhysRevA.86.022711](https://doi.org/10.1103/PhysRevA.86.022711)

PACS number(s): 34.50.Cx, 34.80.Nz, 67.85.-d

I. INTRODUCTION

Samples of cold and ultracold molecules have unique properties that are likely to have applications in many diverse areas. These include high-precision measurement [1,2], quantum information processing [3], and quantum simulation [4]. There is also great interest in the development of controlled ultracold chemistry [5].

Atomic and molecular interactions and collisions are crucial to the production and properties of cold and ultracold molecules. However, quantum-mechanical molecular collision calculations can be computationally extremely expensive. Such calculations are usually carried out using the coupled-channel method, in which the wave function is expanded:

$$\Psi(r, \tau) = r^{-1} \sum_{i=1}^N \varphi_i(\tau) \psi_i(r). \quad (1)$$

Here the N functions $\varphi_i(\tau)$ form a basis set for the motion in all coordinates, τ , except the intermolecular distance, r , and $\psi_i(r)$ is the radial wave function in channel i . Substituting this expansion into the time-independent Schrödinger equation and projecting onto the basis function $\varphi_j(\tau)$ yields a set of N coupled differential equations. The properties of completed collisions are described by the scattering matrix S , which is obtained by matching the functions $\psi_i(r)$ to free-particle wave functions (Ricatti-Bessel functions) at long range [6]. In the full coupled-channel method, explicit solution of the coupled equations takes a time proportional to N^3 .

The problems encountered in cold molecular collisions often require very large numbers of channels. Atom-molecule and molecule-molecule interaction potentials can be strongly anisotropic, requiring large basis sets of rotational functions for convergence. In addition, calculations are often required in an applied field, where the total angular momentum J is no longer a good quantum number [7,8]. Because of this, the large sets of coupled equations cannot be factorized

into smaller blocks for each J as is possible in field-free scattering [9]. Furthermore, at the very low collision energies of interest, small splittings between molecular energy levels have important consequences. Effects such as tunneling [10] and nuclear hyperfine splitting [11,12] multiply the number of channels.

In cold collision studies, the scattering S matrix is often a fast function of collision energy E and magnetic field B , with extensive structure due to scattering resonances and discontinuous behavior at threshold. Calculations are often required over a fine grid of energies and/or applied electric and magnetic fields, and this further multiplies the computational expense.

We have recently shown [13] that multichannel quantum defect theory (MQDT) [14–19] provides an attractive alternative to full coupled-channel calculations in these circumstances. MQDT attempts to represent the scattering properties in terms of a matrix $Y(E, B)$ [16–19] that is a smooth function of E and B . If this can be achieved, the matrix can be obtained once and then used for calculations over a wide range of energies and fields, or obtained by interpolation from a few points. Once the matrix $Y(E, B)$ has been obtained, the time required for calculations at additional energies and fields is only proportional to N , not N^3 .

One problem with MQDT is that the Y matrix may have poles as a function of E and B , and these limit the range over which it can be interpolated. In cold molecular collision studies, calculations are typically needed over an energy range of order 1 K above threshold and for magnetic fields up to a few thousand gauss [20]. This contrasts with the situation for collisions of ultracold atoms, where the energy range of interest is commonly a few μ K and the fields are typically a few hundred gauss.

In the present paper, we show how MQDT Y matrices can be defined to allow smooth interpolation over substantial ranges of collision energy and applied field. This will allow

the use of MQDT to provide substantial savings in computer time.

II. THEORY

A full description of MQDT has been given previously [14–19]. We give here only a brief description, following Ref. [13], which is sufficient to describe the notation we use.

MQDT defines the matrix $Y(E, B)$ at a matching distance r_{match} at relatively short range. The N -channel scattering problem at energy E is partitioned into N_o open channels (with $E_i^\infty \leq E$, where E_i^∞ is the threshold of channel i), N_c weakly closed channels, and N_s strongly closed channels. Strongly closed channels are those that make no significant contribution to the scattering dynamics at $r > r_{\text{match}}$.

The scattering dynamics beyond r_{match} is accounted for using single-channel (uncoupled) calculations in a basis set that diagonalizes the Hamiltonian at $r = \infty$. The solution of the multichannel Schrödinger equation at $r > r_{\text{match}}$ is written in the matrix form

$$\Psi = r^{-1}[\mathbf{f}(r) + \mathbf{g}(r)\mathbf{Y}], \quad (2)$$

where \mathbf{f} and \mathbf{g} are diagonal matrices containing the functions f_i and g_i , which are linearly independent solutions of a reference Schrödinger equation in each asymptotic channel i ,

$$\left[-\frac{\hbar^2}{2\mu} \frac{d^2}{dr^2} + U_i^{\text{ref}}(r) - E \right] f_i(r) = 0, \quad (3)$$

and similarly for $g_i(r)$. The reference potentials $U_i^{\text{ref}}(r)$ approach the true potential at long range, and μ is the reduced mass. They include the centrifugal terms $\hbar^2 L_i(L_i + 1)/2\mu r^2$, where L_i is the partial-wave quantum number for channel i . \mathbf{Y} is an $N_{\text{ref}} \times N_{\text{ref}}$ matrix, where $N_{\text{ref}} = N_o + N_c$.

In our approach [13], \mathbf{Y} is obtained numerically by matching the solutions of the coupled-channel equations to $f_i(r)$ and $g_i(r)$ at r_{match} . The \mathbf{S} matrix is then obtained from \mathbf{Y} using Eqs. (21) to (23) of Ref. [13], which require three QDT parameters (C_i , $\tan \lambda_i$, and ξ_i) in each open channel and a single QDT parameter $\tan \nu_i$ in each weakly closed channel. In the open channels the reference functions are asymptotically

related to Riccati-Bessel functions $J_{L_i}(r)$ and $N_{L_i}(r)$ [6],

$$\begin{pmatrix} f_i \\ g_i \end{pmatrix} = \begin{pmatrix} C_i & 0 \\ -C_i \tan \lambda_i & C_i^{-1} \end{pmatrix} \begin{pmatrix} \cos \xi_i & \sin \xi_i \\ -\sin \xi_i & \cos \xi_i \end{pmatrix} \begin{pmatrix} J_{L_i} \\ N_{L_i} \end{pmatrix}. \quad (4)$$

Here ξ_i is the asymptotic phase shift of the function f_i with respect to the Riccati-Bessel function J_{L_i} . The QDT parameter C_i relates the amplitudes of the energy-normalized functions at long range to functions with Wentzel-Kramers-Brillouin (WKB) normalization at short range, while $\tan \lambda_i$ describes the modification of the WKB phase due to threshold effects. Far from threshold, $C_i \approx 1$ and $\tan \lambda_i \approx 0$. In the weakly closed channels the reference functions are asymptotically

$$\begin{pmatrix} f_i \\ g_i \end{pmatrix} = \begin{pmatrix} \cos \nu_i & \sin \nu_i \\ -\sin \nu_i & \cos \nu_i \end{pmatrix} \begin{pmatrix} \phi_i \\ \gamma_i \end{pmatrix}, \quad (5)$$

where ϕ_i is the solution of Eq. (3) that decays exponentially at large r and γ_i is its linearly independent partner, which is exponentially growing.

The absolute phases chosen for the reference functions f_i and g_i are arbitrary, and different choices produce different \mathbf{Y} matrices and different MQDT parameters. In particular, Eq. (2) shows that a pole in \mathbf{Y} occurs whenever the propagated multichannel wave function in any channel i is proportional to the reference function g_i and has no contribution from f_i . However, all phase choices produce the same physical \mathbf{S} matrix. We are therefore free to choose the phase in order to produce a \mathbf{Y} matrix with advantageous characteristics. Here we show how the phase may be chosen to produce a \mathbf{Y} matrix that is pole free over a wide range of energy or magnetic field and can be interpolated smoothly.

Rotating the reference functions f_i and g_i by an angle θ_i gives a new set of linearly independent reference functions \bar{f}_i and \bar{g}_i ,

$$\begin{pmatrix} \bar{f}_i \\ \bar{g}_i \end{pmatrix} = \begin{pmatrix} \cos \theta_i & -\sin \theta_i \\ \sin \theta_i & \cos \theta_i \end{pmatrix} \begin{pmatrix} f_i \\ g_i \end{pmatrix}. \quad (6)$$

These rotated reference functions define a new \mathbf{Y} matrix and a new set of QDT parameters (\bar{C} , $\tan \bar{\lambda}$, $\bar{\xi}$, and $\tan \bar{\nu}$). Combining Eqs. (4), (5), and (6) gives

$$\bar{\xi}_i = \arctan \left[\frac{C_i^2 \sin \xi_i (\cos \theta_i + \tan \lambda_i \sin \theta_i) - \cos \xi_i \sin \theta_i}{C_i^2 \cos \xi_i (\cos \theta_i + \tan \lambda_i \sin \theta_i) + \sin \xi_i \sin \theta_i} \right], \quad (7)$$

$$\tan \bar{\lambda}_i = -\frac{2C_i^4 \tan \lambda_i \cos 2\theta_i + [1 + C_i^4 (\tan^2 \lambda_i - 1)] \sin 2\theta_i}{2\{C_i^4 \cos^2 \theta_i + \sin \theta_i [\sin \theta_i + C_i^4 \tan \lambda_i (2 \cos \theta_i + \tan \lambda_i \sin \theta_i)]\}}, \quad (8)$$

$$\bar{C}_i = \left[\frac{\sin \xi_i \sin \theta_i}{C_i} + C_i \cos \xi_i (\cos \theta_i + \tan \lambda_i \sin \theta_i) \right] \sqrt{1 + \frac{[\cos \xi_i \sin \theta_i - C_i^2 \sin \xi_i (\cos \theta_i + \tan \lambda_i \sin \theta_i)]^2}{[\sin \xi_i \sin \theta_i + C_i^2 \cos \xi_i (\cos \theta_i + \tan \lambda_i \sin \theta_i)]^2}}, \quad (9)$$

$$\bar{\nu}_i = \nu_i - \theta_i. \quad (10)$$

Far from threshold ($E \gg 1$ K), Eqs. (7) to (10) simplify to $\bar{\xi}_i = \xi_i - \theta_i$, $\tan \bar{\lambda}_i \approx 0$, $\bar{C}_i \approx 1$, and $\bar{\nu}_i = \nu_i - \theta_i$. However, in the threshold region that is of interest in cold molecule studies, Eqs. (7) to (10) must be evaluated explicitly.

A. Basis sets and quantum numbers

As a test case, we consider cold collisions between NH ($^3\Sigma^-$) and Mg atoms [21]. This is the same system as considered in Ref. [13], but the present work uses a larger

basis set, which introduces more scattering resonances and denser poles in the \mathbf{Y} matrix.

The energy levels of NH in a magnetic field are most conveniently described using Hund's case (b), in which the molecular rotation n couples to the spin s to produce a total monomer angular momentum j . In zero field, each rotational level n is split into sublevels labeled by j . In a magnetic field, each sublevel splits further into $2j + 1$ levels labeled by m_j , the projection of j onto the axis defined by the field. For the $n = 0$ levels that are of most interest for cold molecule studies, there is only a single zero-field level with $j = 1$ that splits into three components with $m_j = +1, 0$, and -1 .

The coupled equations are constructed in a partly coupled basis set $|n s j m_j\rangle |L M_L\rangle$, where L is the end-over-end rotational angular momentum of the Mg atom and the NH molecule about one another and M_L is its projection on the axis defined by the magnetic field. Hyperfine structure is neglected. The matrix elements of the total Hamiltonian in this basis set are given in Refs. [8] and [22]. The only good quantum numbers during the collision are the parity $p = (-1)^{n+L+1}$ and the total projection quantum number $M = m_j + M_L$. The calculations in the present work are performed for $p = -1$ and $M = 1$. This choice includes s-wave scattering of NH molecules in initial state $m_j = +1$, which is magnetically trappable, to $m_j = 0$ and -1 , which are not. The present work uses a converged basis set including all functions up to $n_{\max} = 6$ and $L_{\max} = 8$, as in Ref. [21].

We label elements of \mathbf{Y} and \mathbf{S} by subscripts $\alpha, L, M_L \rightarrow \alpha', L', M'_L$, where α represents an eigenstate of free NH that may be approximately labeled by (n, s, j, m_j) . However, the collisions considered in the present paper are all among the $n = 0, j = 1$ levels and so α is simply abbreviated to m_j . For diagonal elements we suppress the second set of labels.

B. Numerical methods

The coupled-channel calculations required for both MQDT and the full coupled-channel approach were carried out using the MOLSCAT package [23], as modified to handle collisions in magnetic fields [22]. The coupled equations were solved numerically using the hybrid log-derivative propagator of Alexander and Manolopoulos [24], which uses a fixed-step-size log-derivative propagator in the short-range region ($r_{\min} \leq r < r_{\text{mid}}$) and a variable-step-size Airy propagator in the long-range region ($r_{\text{mid}} \leq r \leq r_{\max}$). The full coupled-channel calculations used $r_{\min} = 2.5 \text{ \AA}$, $r_{\text{mid}} = 50 \text{ \AA}$, and $r_{\max} = 250 \text{ \AA}$ (where $1 \text{ \AA} = 10^{-10} \text{ m}$). MQDT requires coupled-channel calculations only from r_{\min} to r_{match} (which is less than r_{mid}), so only the fixed-step-size propagator was used in this case.

The MQDT reference functions and quantum defect parameters were obtained as described in Ref. [13], using the renormalized Numerov method [25] to solve the one-dimension Schrödinger equations for the reference potentials. The MQDT \mathbf{Y} matrix was then obtained by matching to the log-derivative matrix extracted from the coupled-channel propagation at a distance r_{match} . In this paper all MQDT calculations use the reference potential

$$U_i^{\text{ref}}(r) = V_0(r) + \frac{\hbar^2 L_i(L_i + 1)}{2\mu r^2} + E_i^\infty, \quad (11)$$

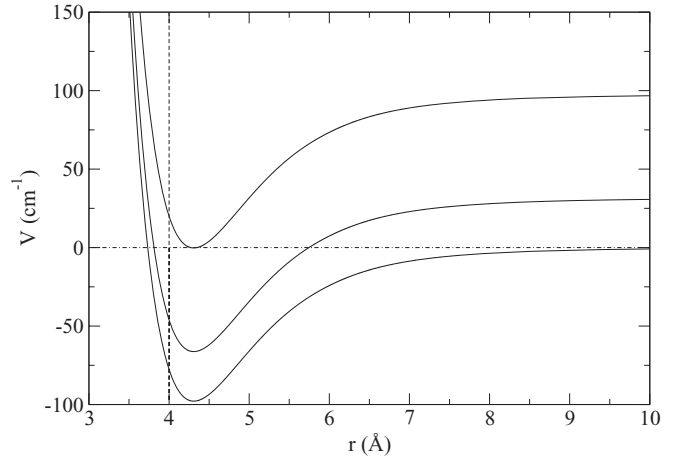


FIG. 1. The V_0 reference potentials for Mg + NH. The first and second rotational excited states are also shown ($n = 1, 2$). The hard wall at $r = 4.0 \text{ \AA}$ is shown as a vertical dashed line. The dot-dashed horizontal line corresponds to zero energy.

where $V_0(r)$ is the isotropic part of the interaction potential. This reference potential has been shown to produce quantitatively accurate results when \mathbf{Y} is re-evaluated at each collision energy and magnetic field [13]. However, such re-evaluation relinquishes most of the computational savings that MQDT is intended to achieve.

The reference potential contains a hard wall at $r = r_i^{\text{wall}}$, so that $U_i^{\text{ref}}(r) = \infty$ for $r < r_i^{\text{wall}}$. In the present paper we take $r_i^{\text{wall}} = 4.0 \text{ \AA}$. Figure 1 shows the reference potentials for the lowest three rotational states. All channels with $n \geq 2$ were treated as strongly closed and thus not included in the MQDT part of the calculation, but were included in the log-derivative propagation.

III. RESULTS AND DISCUSSION

Figure 2(a) shows a single diagonal element of the \mathbf{Y} matrix, $Y_{-1,8+2}$, as a function of the matching distance and energy, obtained with unrotated reference functions. $Y_{-1,8+2}$ is a representative element of \mathbf{Y} with poles at the same locations as the other elements, chosen to give a good visual representation of the pole structure. There are many poles visible, which prevent polynomial interpolation over energies of more than 0.5 K for any value of r_{match} (and much less than this for some choices of r_{match}). The energies of the poles become independent of r_{match} at long range.

The presence of low-energy poles in \mathbf{Y} for some values of r_{match} is a serious problem. For MQDT to be efficient, r_{match} must be chosen *without* solving the coupled equations at many different energies. The calculations needed to produce contour plots such as those in Fig. 2 are feasible for a test case such as Mg + NH, but would be prohibitively expensive for a very large system.

Figure 2(b) shows the same element of the \mathbf{Y} matrix as a function of the matching distance and energy for reference functions rotated by $\theta_i = \pi/2$. The poles are in quite different places, but once again there are many of them. The combination of Figs. 2(a) and 2(b) demonstrates that, for any arbitrary choice of rotation angles, poles will appear in the

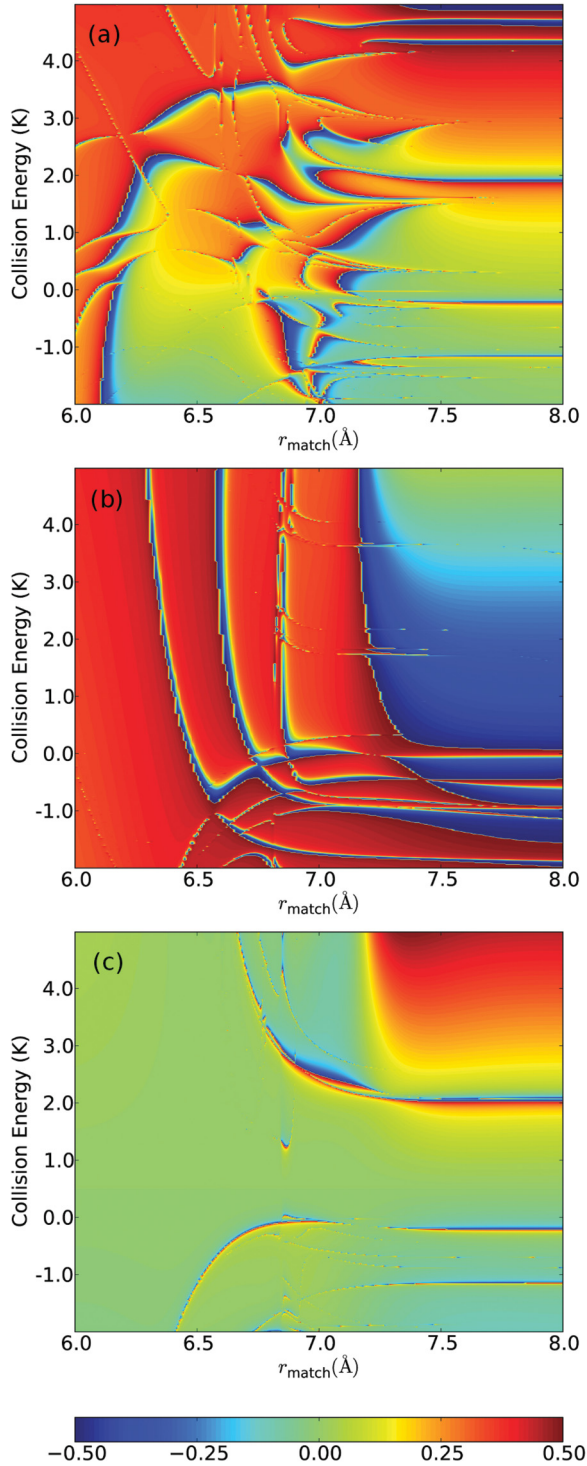


FIG. 2. (Color online) Contour plot of $\arctan Y_{ii}/\pi$ for a representative diagonal \mathbf{Y} matrix element, $Y_{-1,8,+2}$, as a function of energy and r_{match} at $B = 10$ G: (a) obtained with unrotated reference functions ($\theta_i = 0$), (b) obtained with reference functions rotated by $\theta_i = \pi/2$, and (c) obtained with optimized reference functions with $\theta_i = \theta_i^{\text{opt}}$ in all channels. The arctangent is shown for clarity of plotting: It maps the real numbers, \mathbb{R} , to the domain $-\pi/2$ to $\pi/2$, thus allowing all magnitudes of \mathbf{Y} matrix elements to be seen on a single plot.

\mathbf{Y} matrix, preventing simple interpolation for most choices of r_{match} . This will be true in any MQDT problem with a large

density of resonances. The contour plots do, however, show that the position of poles is strongly dependent on the rotation angle, even at large values of r_{match} . This suggests that it will be possible to optimize the rotation angles in order to move the poles away from the energy range of interest. It is emphasized that the \mathbf{S} matrices obtained from the \mathbf{Y} matrices shown in the different panels of Fig. 2 are identical.

We now consider how to rotate the reference functions to maximize the pole-free range over which \mathbf{Y} can be interpolated. Y_{ii} as a function of θ_i is given by

$$Y_{ii} = \tan(\theta_i + \delta_i), \quad (12)$$

where δ_i is the phase shift between the unrotated reference function f_i and the propagated multichannel wave function in channel i . There is a pole in Y_{ii} when $\theta_i + \delta_i = \pi/2$ and a zero when $\theta_i + \delta_i = 0$. We thus set $\theta_i^{\text{opt}} = -\delta_i$ at one choice of r_{match} , E and B , so that the propagated multichannel wave function and the reference wave functions are almost in phase and the resulting \mathbf{Y} matrix in that region is pole free.

Because the channels are coupled, rotating the reference functions in one channel affects the other elements of the \mathbf{Y} matrix. In this work we loop over the channels sequentially, setting each diagonal element to 0 in turn. By repeatedly looping over all channels, all the diagonal \mathbf{Y} matrix elements are set to 0. For Mg + NH it was sufficient to loop over the channels twice. In a more strongly coupled system it is expected that this would need to be repeated more times. This approach allows a set of optimized θ_i to be obtained from a single multichannel propagation.

Rotated reference functions have previously been used to transform \mathbf{Y} matrices in the study of atomic spectra [26–30] and atomic collisions [31]. Adjusting θ_i at each energy such that $Y_{ii} = 0$ was shown to produce a weak energy dependence of off-diagonal \mathbf{Y} matrix elements across thresholds [31]. However, this approach required propagating the full multichannel wave function many times at different energies, which is precisely what the present work tries to avoid.

Figure 2(c) shows how the representative element $Y_{-1,8,+2}^{\text{opt}}$ varies as a function of the matching distance and energy. All the θ_i values are optimized as described above at $E = 0.5$ K and $B = 10$ G for each value of r_{match} , but are *not* reoptimized at each energy. Comparison of this with Figs. 2(a) and 2(b) shows the effectiveness of optimizing the reference functions. Without optimization, there were no choices of r_{match} for which \mathbf{Y} was pole free and thus suitable for interpolation over the energy range of interest. After optimization, \mathbf{Y}^{opt} is pole free over a substantial range, of about 1 K, for any choice of $r_{\text{match}} < 8$ Å. For values of $r_{\text{match}} < 6.5$ Å, \mathbf{Y}^{opt} is pole free over many Kelvin. Beyond 6.5 Å, poles start to enter \mathbf{Y}^{opt} in the energy range of interest. Once the poles have settled at their asymptotic values at $r_{\text{match}} > 7.5$ Å, we find that positive energies up to about 2 K are pole free. However, at larger values of r_{match} the linearity of \mathbf{Y}^{opt} over the pole-free region decreases. This is due to negative-energy poles in the \mathbf{Y} matrix, which our procedure cannot move significantly. There is one particularly bad choice of r_{match} at about 6.8 Å, but provided this unlucky choice of r_{match} is avoided, \mathbf{Y}^{opt} can be interpolated smoothly over the positive energy range from 0 to > 2 K for any choice of r_{match} .

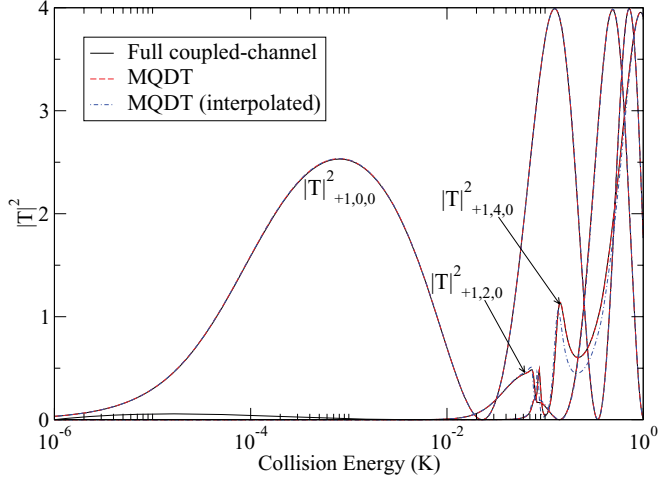


FIG. 3. (Color online) The squares of diagonal T -matrix elements T_{m_j, L, M_L} in the incoming channels for $m_j = +1$ and $L = 0, 2$, and 4 at $B = 10$ G, obtained from full coupled-channel calculations (solid, black) and MQDT with optimized reference functions for $r_{\text{match}} = 6.5$ Å, both with (dot-dash, blue) and without (dashed, red) interpolation.

Figure 3 compares diagonal T -matrix elements $|T_{ii}|^2$ (where $T_{ij} = \delta_{ij} - S_{ij}$) obtained from full coupled-channel calculations with those from the MQDT method, with a matching distance of $r_{\text{match}} = 6.5$ Å, using reference functions optimized at 0.5 K. MQDT results were obtained both by recalculating the Y matrix at every energy and by interpolating Y^{opt} linearly between two points separated by 1 K. The MQDT results with Y recalculated at each energy can scarcely be distinguished from the full coupled-channel results. The MQDT results obtained by interpolation are also very similar to the full coupled-channel results except around the resonance feature at $E \approx 0.1$ K. The interpolated result could, of course, be improved simply by performing coupled-channel calculations to obtain Y^{opt} at one or two extra energies across the range, to allow for a higher-order interpolation, or by using a linear interpolation over a smaller energy range.

In this work we use θ_i to rotate our short-range reference functions f_i and g_i . In principle, we could rotate the reference functions by varying the asymptotic phase shifts $\bar{\xi}_i$ instead of the short-range phases θ_i . However, Figure 4 shows why this is not desirable. Due to the highly nonlinear relationship between $\bar{\xi}_i$ and θ_i , obtaining the optimum rotation angle of the short-range reference functions f_i and g_i by varying the angle $\bar{\xi}_i$ would be laborious at very low collision energies.

A. Magnetically tunable Feshbach resonances

The effects of magnetic fields on cold molecular collisions are very important, since collisions can be controlled by taking advantage of magnetically tunable low-energy Feshbach resonances. We are therefore interested in how S matrix elements behave as a function of magnetic field across Feshbach resonances. It is thus important that the Y matrix is weakly dependent on magnetic field in such regions.

Figure 5 shows the diagonal elements of the optimized Y matrix as a function of magnetic field for Mg + NH collisions over the range from 10 to 5000 G for a collision energy of 1 mK.

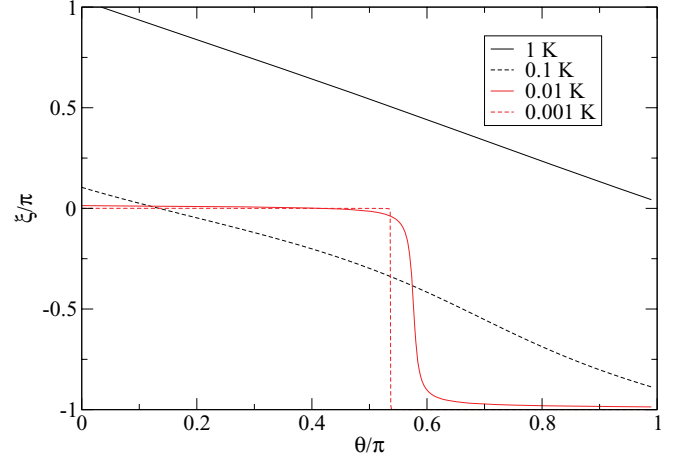


FIG. 4. (Color online) The asymptotic phase shift $\bar{\xi}_i$ as a function of the rotation angle θ_i for the incoming d -wave channel $(+1, 2, 0)$.

This range of fields tunes across six Feshbach resonances. The reference functions were optimized at 10 G and 1 mK. The elements of Y^{opt} are smoothly curved over the entire 5000-G range and could be well represented by a low-order polynomial.

Figure 6 shows the comparison between optimized MQDT and full coupled-channel calculations for a selection of diagonal and off-diagonal T -matrix elements as the magnetic field is tuned at 1 mK. The reference functions were optimized at 10 G and 1 mK and MQDT results were obtained by linear interpolation of Y^{opt} between two points separated by 1000 G and by 5000 G. Interpolation over 1000 G gives resonance features that are in very good agreement with the full coupled-channel calculation to better than 1 G. Interpolation over 5000 G gives resonance features of the correct shape, with positions that are still within about 10 G of the full coupled-channel results. The difference between the interpolated result and the full coupled-channel calculation is a result of both the choice of r_{match} and the interpolation. The quality of the interpolation could be improved by considering a few more fields across the range to allow for higher-order polynomial

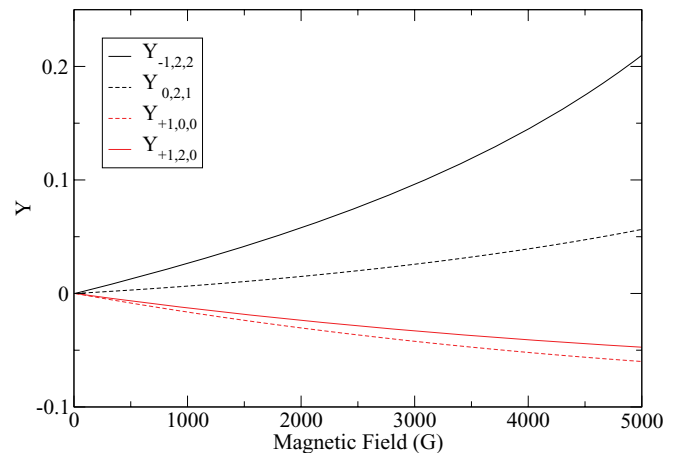


FIG. 5. (Color online) Representative Y^{opt} matrix elements as a function of field at $E = 1$ mK.

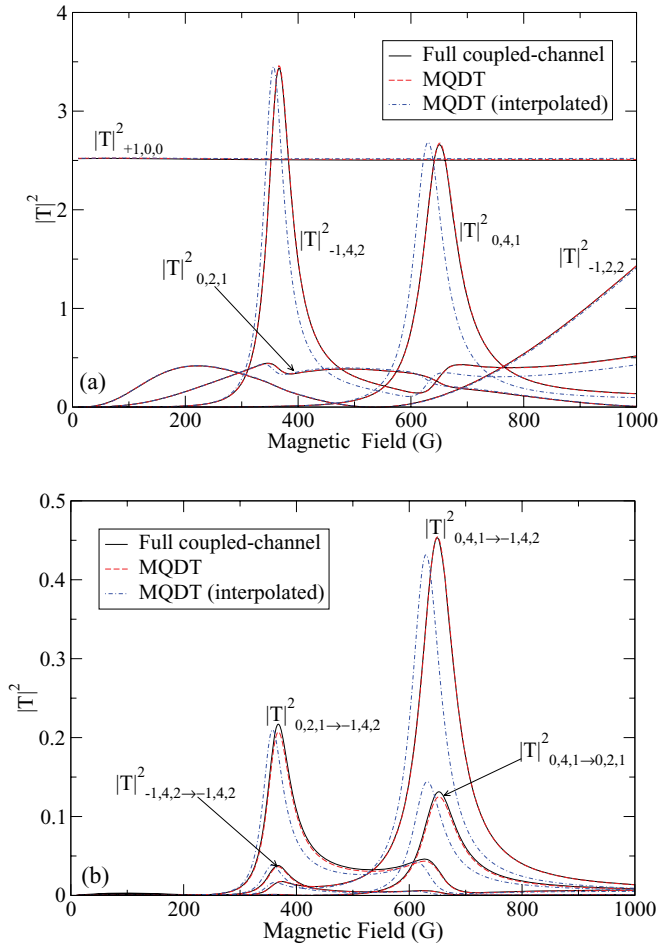


FIG. 6. (Color online) Squares of T -matrix elements at 1 mK as a function of field in the vicinity of a Feshbach resonance: (a) diagonal elements and (b) off-diagonal elements.

interpolation or by using linear interpolation over a smaller field range.

Full MQDT calculations recalculating the Y matrix at every magnetic field give resonance positions accurate to 0.4 G. The remaining errors between the full coupled-channel calculations and the MQDT results will reduce with a larger value of r_{match} . As seen in Figure 2(c), the optimized Y matrices obtained at larger values of r_{match} are still amenable to interpolation, though over a more restricted energy range.

IV. CONCLUSIONS

We have shown that multichannel quantum defect theory can provide an efficient computational method for low-energy

molecular collisions as a function of both energy and magnetic field. In particular, we have shown how a disposable parameter of MQDT, the phase of the short-range reference functions, may be chosen to make the MQDT Y matrix smooth and pole free over a wide range of energy and field. This smooth variation allows the Y matrix to be evaluated from coupled-channel calculations at a few values of the energy and field and then to be obtained by interpolation at intermediate values. It is not necessary to repeat the expensive coupled-channel part of the calculation on a fine grid.

The procedure developed here is to choose the phase of the reference functions in each channel so that the diagonal Y matrix in each channel is zero at a reference energy and field. This ensures that there are no poles in the Y matrix, which would prevent smooth interpolation, close to the reference energy. Optimizing the phase in this way is very inexpensive, and once it is done the cost of calculations at additional energies and fields varies only linearly with the number of channels N , not as N^3 as for full coupled-channel calculations. MQDT with optimized Y matrices is thus a very promising alternative to full coupled-channel calculations for cold molecular collisions, particularly when fine scans over collision energy and magnetic field are required.

The Y matrix is defined to encapsulate all the collision dynamics that occurs inside a matching distance r_{match} , and the choice of this distance is important. There is a trade-off between the accuracy of the method and the size of the pole-free region of the optimized Y matrix. For large values of r_{match} , resonant features may appear in the Y matrix and prevent simple interpolation over large ranges of energy and field. For smaller values of r_{match} , optimizing the reference functions allows interpolation over many Kelvin, but the accuracy of MQDT is reduced because interchannel coupling is neglected outside r_{match} .

For the moderately anisotropic Mg + NH system studied here, optimized MQDT with an interpolated Y matrix can provide numerical results in quantitative agreement with fully converged coupled-channel calculations. In future work, we will investigate the extension of this approach to more strongly coupled systems, with larger anisotropy of the interaction potential and more closed channels that produce scattering resonances.

ACKNOWLEDGMENTS

The authors are grateful for support from EPSRC, AFOSR MURI Grant No. FA9550-09-1-0617, and EOARD Grant No. FA8655-10-1-3033.

[1] J. J. Hudson, B. E. Sauer, M. R. Tarbutt, and E. A. Hinds, *Phys. Rev. Lett.* **89**, 023003 (2002).
 [2] H. L. Bethlem and W. Ubachs, *Faraday Discuss.* **142**, 25 (2009).
 [3] D. DeMille, *Phys. Rev. Lett.* **88**, 067901 (2002).
 [4] L. D. Carr, D. DeMille, R. V. Krems, and J. Ye, *New J. Phys.* **11**, 055049 (2009).

[5] R. V. Krems, *PhysChemChemPhys* **10**, 4079 (2008).
 [6] B. R. Johnson, *J. Comput. Phys.* **13**, 445 (1973).
 [7] A. Volpi and J. L. Bohn, *Phys. Rev. A* **65**, 052712 (2002).
 [8] R. V. Krems and A. Dalgarno, *J. Chem. Phys.* **120**, 2296 (2004).
 [9] A. M. Arthurs and A. Dalgarno, *Proc. R. Soc., Ser. A* **256**, 540 (1960).

- [10] P. S. Żuchowski and J. M. Hutson, *Phys. Rev. A* **79**, 062708 (2009).
- [11] M. Lara, J. L. Bohn, D. E. Potter, P. Soldán, and J. M. Hutson, *Phys. Rev. A* **75**, 012704 (2007).
- [12] M. L. González-Martínez and J. M. Hutson, *Phys. Rev. A* **84**, 052706 (2011).
- [13] J. F. E. Croft, A. O. G. Wallis, J. M. Hutson, and P. S. Julienne, *Phys. Rev. A* **84**, 042703 (2011).
- [14] M. J. Seaton, *Proc. Phys. Soc.* **88**, 801 (1966).
- [15] M. J. Seaton, *Rep. Prog. Phys.* **46**, 167 (1983).
- [16] C. H. Greene, A. R. P. Rau, and U. Fano, *Phys. Rev. A* **26**, 2441 (1982).
- [17] F. H. Mies and P. S. Julienne, *J. Chem. Phys.* **80**, 2526 (1984).
- [18] F. H. Mies and M. Raoult, *Phys. Rev. A* **62**, 012708 (2000).
- [19] M. Raoult and F. H. Mies, *Phys. Rev. A* **70**, 012710 (2004).
- [20] Units of gauss rather than tesla, the accepted SI unit of magnetic field, are used in this paper to conform to the conventional usage of this field.
- [21] A. O. G. Wallis and J. M. Hutson, *Phys. Rev. Lett.* **103**, 183201 (2009).
- [22] M. L. González-Martínez and J. M. Hutson, *Phys. Rev. A* **75**, 022702 (2007).
- [23] J. M. Hutson and S. Green, MOLSCAT computer program, version 14, distributed by Collaborative Computational Project No. 6 of the UK Engineering and Physical Sciences Research Council (Daresbury, 1994).
- [24] M. H. Alexander and D. E. Manolopoulos, *J. Chem. Phys.* **86**, 2044 (1987).
- [25] B. R. Johnson, *J. Chem. Phys.* **67**, 4086 (1977).
- [26] A. Giusti-Suzor and U. Fano, *J. Phys. B* **17**, 215 (1984).
- [27] A. Giusti-Suzor and U. Fano, *J. Phys. B* **17**, 4267 (1984).
- [28] A. Giusti-Suzor and U. Fano, *J. Phys. B* **17**, 4277 (1984).
- [29] W. E. Cooke and C. L. Cromer, *Phys. Rev. A* **32**, 2725 (1985).
- [30] W. Eissner, H. Nussbaumer, H. E. Saraph, and M. J. Seaton, *J. Phys. B* **2**, 341 (1969).
- [31] R. Osséni, O. Dulieu, and M. Raoult, *J. Phys. B* **42**, 185202 (2009).